Role of ion density in growth, transport, and morphology of nanoparticles generated in plasmas

Kil Byoung Chai and Wonho Choe
Department of Physics, Korea Advanced Institute of Science and Technology, 291 Daehak-ro, Yuseong-gu, Daejeon 305-701, South Korea

(Received 30 April 2012; accepted 1 August 2012; published online 20 August 2012)

Spatial distribution, growth, and morphology of the nanoparticle were investigated in the plasmas with relatively low and high ion densities. Our experimental results reveal that cauliflower-shaped amorphous nanoparticles are dominantly distributed throughout the entire plasma in the low ion density plasma while spherical crystalline particles are spread near the plasma edge in the high ion density plasma. Only agglomeration growth step of the nanoparticles was observed without molecular accretion growth step in the high density plasma. Based on the experimental and numerical results, the role of ion density in the growth mechanism and transport of the nanoparticles is discussed. © *2012 American Institute of Physics*. [http://dx.doi.org/10.1063/1.4746396]

Dusty plasmas containing small solid particles as well as electrons and ions have been widely studied over the years in a variety of plasmas including space plasmas, dusty plasma crystals, and high temperature tokamak plasmas.[1–3] Also, there have been a number of recent attempts and efforts to develop practical applications of dusty plasmas to the semiconductor and solar cell industries.[4]

In many research fields, the control of dust particles has become more important and thus has been an active research issue for the last two decades.[5] For instance, the control of trapped position and dynamics of dust particles is critical to investigate phase transition phenomena and wave propagation research.[6] In solar cell and semiconductor industries, highly crystalline nano-sized particle is regarded as a potential candidate for improving the efficiency.[7] The method for removing dust particles is urgently required because dusts cause many safety problems related to the radioactive tritium in high temperature tokamak plasmas.[8]

For control of the generation, transport, and physical properties of the dust particle, understanding of the plasma-dust interactions is prerequisite. Among them, ion-dust interaction has attained a lot of concerns because it is a fundamental process in plasma-dust interactions[9] and it is possible to be used as a control knob of dust characteristics.[10] However, the rigorous study on the role of ion density in the dust generation and growth has been relatively less performed due to the difficulties of diagnostics of both dust particles and the plasma where active chemical reactions occur.

In this paper, we study the role of ion density in generation, growth, and transport of dust particles by comparing the spatial distribution, growth rate, and morphology of the nanoparticle as well as plasma parameters in between low density and high density plasma regimes at the same plasma source. We then quantitatively discuss our experimental results with calculations for obtaining a conclusive knowledge on the role of ion density in the dust generation, transport, and physical properties.

In the experiment, inductively coupled plasmas having a planar-type single-turn antenna of 18 cm in diameter placed on the top of a cylindrical vacuum chamber of 26 cm in diameter and 20 cm in height were used. The detailed chamber configuration is depicted in Ref. 11. The antenna was connected to a 13.56 MHz power generator (RFPP RF10S) through an automatic impedance matcher (RFPP AMNPS-2 A). Plasmas were produced by supplying a gas mixture of 5% SiH_4 and 95% Ar in which silicon-based nanoparticles were generated and grown.

A TEM grid was placed at the side port of the chamber connected to the vacuum pump to collect the nanoparticles, and the size and morphology of the collected particles were obtained by transmission electron microscopy (TEM; Technai T30). A floating probe was installed at 2 cm below the dielectric plate (dielectric plate was placed between the antenna coil and cylindrical chamber) and the radial center of the vacuum chamber which corresponds to the bulk plasma region. The tip of the probe was biased by 50 kHz ac voltage, and the electron temperature and ion flux were obtained by analyzing the first (50 kHz) and second (100 kHz) harmonics of the collected probe current. It is possible to accurately collect the plasma current even if the probe tip becomes coated by a dielectric material inside plasma because ac voltage is applied as opposed to other conventional electrostatic probes.[12]

Laser light scattering was employed to measure the spatial distribution of the generated nanoparticles in which the laser light is projected onto the nanoparticles and the scattered light from them is measured. In this work, a low power (30 mW) He-Ne laser with 2 mm in diameter was utilized as a probe beam, and two spherical mirrors with a focal length of 4 m and reflectivity of 99.9% at 632.8 nm were placed at both sides of the vacuum chamber to have multiple laser beam paths. By properly tilting the mirrors, 7 vertically spread beam paths ranged from 1.0 cm to 3.5 cm from the bottom electrode surface were obtained. In this set up, the intensity of the incident beam did not diminish even if the laser beam was spread vertically,[13] so it was able to distinguish the scattered signal from the plasma emission. A CCD camera (Samsung SHC-740 N) was utilized for measuring the nanoparticle distribution in two dimensions.

 © 2012 American Institute of Physics

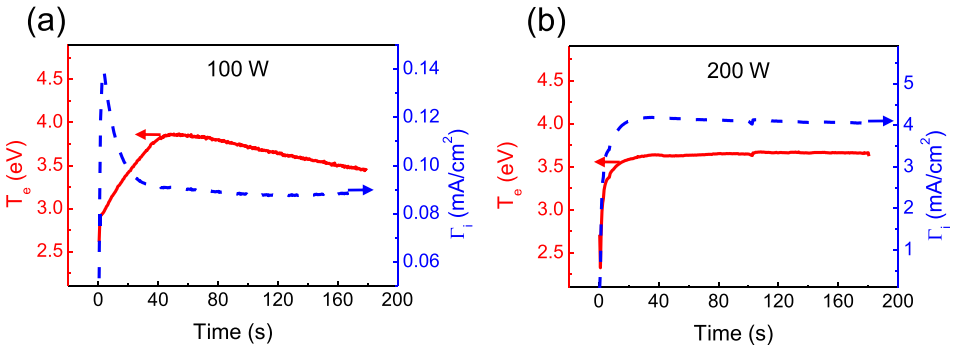

FIG. 1. Time evolution of T_e and Γ_i measured at (a) 100 W (E-mode) and (b) 200 W (H-mode), respectively. Both T_e and Γ_i significantly change in the low n_i regime but stay almost unchanged in the high n_i regime.

In this experiment, two different density regimes were obtained at the same plasma source set up by only raising the input rf power: the E-mode representing the capacitive mode having a relatively low density and the H-mode representing the inductive mode with a relatively high density. The plasma parameters and optical emission intensity were measured at the radial center and 2 cm below the quartz plate as the input rf power was raised and a significant increase in both ion flux Γ_i and 750.4 nm Ar I line intensity by approximately 20 times and 10 times, respectively, was observed at (160–180) W, indicating an E-H mode transition. On the contrary, the electron temperature T_e slightly decreased. Because the Γ_i is proportional to Bohm velocity v_B [$v_B = (ekT_e/M_i)^{1/2}$] (where k is the Boltzmann constant and M_i is the ion mass) and ion density n_i and the difference in T_e between the E-mode and the H-mode is much smaller than that in Γ_i, the difference in Γ_i is mostly attributed to the difference in n_i. We therefore consider the E- and H-modes as low and high ion density regimes, respectively.

The time evolution of the plasma parameters between low density regime (100 W) and high density regime (200 W) is compared, and the results are presented in Fig. 1. Interestingly, both T_e (solid) and Γ_i (dashed) significantly change over time in the low density regime but remain almost constant in the high density regime. Because the nanoparticle immersed in the plasma captures a large amount of electrons and ions, the plasma parameters also change over time following the nanoparticle growth.[11] It is found that the low density regime is more affected by the nanoparticle generation and growth.

Presented in Fig. 2 is the 2-dimensional spatial distribution of the nanoparticles with the input rf power varied from 100 W to 200 W, where (a)–(d) describe the low density regime and (e)–(f) depict the high density regime. It is noted that only the lower part of the plasma was observed due to the port availability. While the nanoparticles represented by bright regions are spread throughout the entire plasma for entire discharge time in the low density regime, they are distributed mainly in the plasma edge in the high density regime (after 30 s).

In order to find out the cause for the different particle distributions between the two regimes, the forces exerted on a 20 nm nanoparticle, which is the representative size of the produced particle under this experiment, are estimated as follows between low density regime (100 W) and high density regime (200 W). For the sake of simplicity, a single isolated

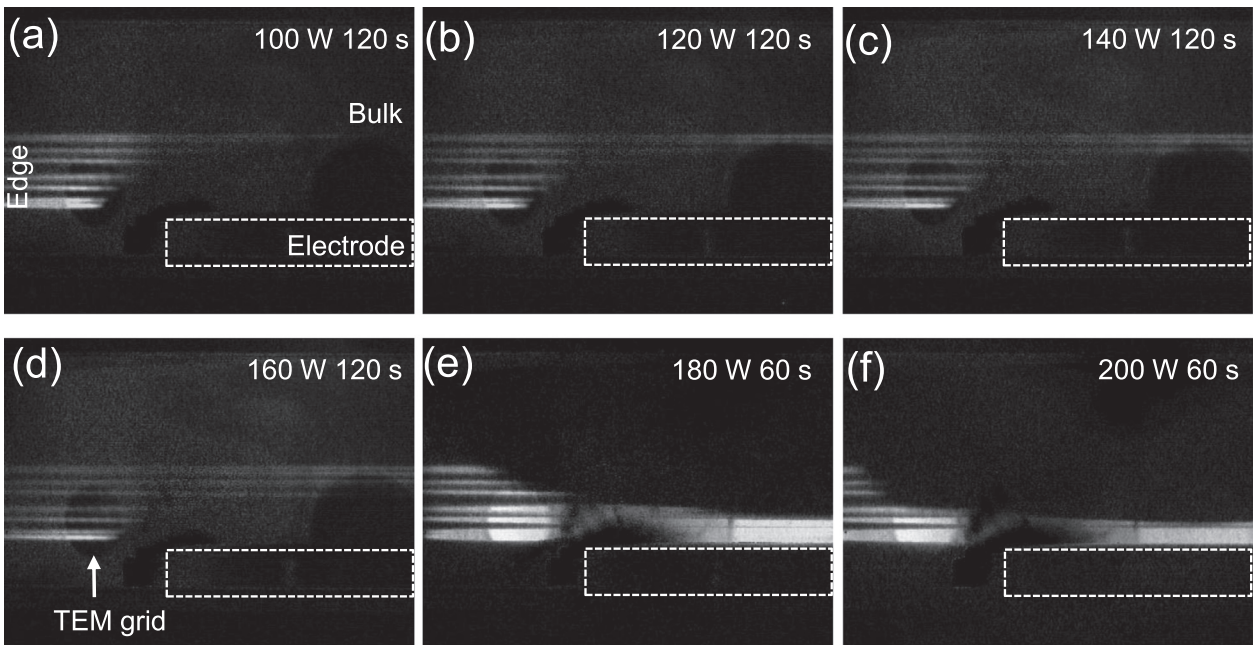

FIG. 2. Two-dimensional distributions of nanoparticles under various rf power conditions. (a)-(d) represent the low n_i and (e)–(f) represent the high n_i regimes. The nanoparticles are distributed throughout the entire plasma region in the low n_i regime while they are spread throughout the edge region in the high n_i regime.

nanoparticle is assumed to be immersed in the plasma. The electrostatic force exerted on the particle is $F_{es} = eZ_pE_0$, where e is the elementary charge and E_0 is the internal ambipolar electric field. The charge number of the nanoparticle Z_p obtained from the relation for the argon plasma is analytically expressed as[14]

$$Z_p = 0.73\frac{4\pi\varepsilon_0 r_p kT_e}{e^2}\ln\left[\frac{n_i}{n_e}\left(\frac{m_eT_i}{m_iT_e}\right)^{1/2}\right], \quad (1)$$

where $\varepsilon_0 = 8.854\times10^{-12}$ F/m, r_p is the nanoparticle radius in m, T_i is the ion temperature, n_e is the electron density, and m_e is the electron mass. With measured values and $kT_i = 0.03$ eV, the charge number Z_p of a 20 nm particle was 100 for both regimes. The potential energy difference between the plasma center and the sheath edge is roughly $kT_e/2$ and the radial length of the bulk region is about 0.1 m. Thus, the average ambipolar electric field can be estimated for both regimes 20 V/m. Consequently, $F_{es} = 4.0\times10^{-16}$ N for both low and high density regimes.

The ion drag exerted on a particle is given by[15]

$$F_{id} = \pi r_p^2 n_i m_i u_i^2\left(1-\frac{2e\phi_p}{m_iu_i^2}\right) + \frac{\pi}{2}\ln\left(1+\frac{4}{b^2}\lambda_{DL}^2\right)n_im_iu_i^2b^2G(\chi,\zeta), \quad (2)$$

where u_i is the ion drift speed, ϕ_p is the floating potential of the nanoparticle, λ_{DL} is the linearized Debye length, and $b = Z_pe^2/2\pi\varepsilon_0m_iu_i^2$. Here, $G(\chi, \zeta)$ is the correction function which is given by[15]

$$G(\chi,\zeta) = \left[\sqrt{\pi}\ln\left(1+\frac{\chi^4}{\zeta^2}\right)\right]^{-1} \times\int_0^\infty\frac{2\chi x\cosh(2\chi x)-\sinh(2\chi x)}{x^2} \times\ln\left(1+\frac{\chi^4}{\zeta^2}\right)\exp[-(x^2+\chi^2)]dx, \quad (3)$$

where $\chi = u_i/v_{th,i}$ and $\zeta = -r_p2e\phi_p/\sqrt{61.32}\lambda_{DL}m_iv_{th,i}^2$. This term is necessary when the ion drift speed u_i is smaller than the ion thermal speed $v_{th,i}$ ($\chi < 1$). Because the measured densities and temperatures satisfy $\mu_e \gg \mu_i$ and $T_e \gg T_i$, the ion drift speed u_i can be expressed as $u_i = \mu_iE_0$ (Ref. 16) where μ_i and μ_e are the ion and electron mobilities ($\mu_s = e/m_s\nu_{sn}$, where $s = e, i$, and ν_{sn} is the s-neutral collision frequency). Using the measured kT_e and Γ_i, the ion drag exerted on a 20 nm radius nanoparticle is calculated as $F_{id} = 2.9\times10^{-16}$ N for the 100 W case and $F_{id} = 1.9\times10^{-15}$ N for the 200 W case. The gravity is negligible for this size of the particle. Therefore, the estimated forces indicate that F_{es} (inward) $> F_{id}$ (outward) in the low density regime and F_{es} (inward) $\ll F_{id}$ (outward) in the high density regime. This result agrees well with the experimentally observed nanoparticle distribution in the plasma.

Figure 3 reveals the time evolution of nanoparticle radius in both low and high density regimes studied by TEM images. There are two points should be noted: the particle

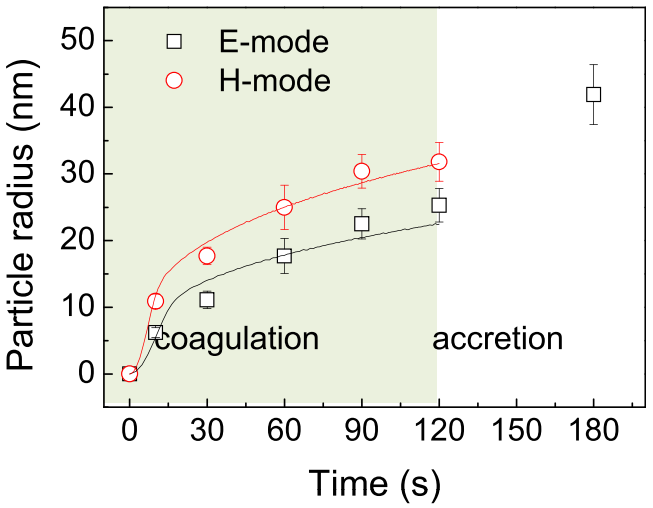

FIG. 3. Nanoparticle growth rate in the low n_i (square) and high n_i regimes (circle). While the nanoparticle size gradually increases in the relatively low n_i regime, it saturates at about 30 nm in the high n_i regime.

growth rate in the high density regime is larger than that in the low density regime during the agglomeration period (early discharge phase) and the continuous growth (particles are still growing even after 180 s) of the particle is seen in the molecular accretion period (late discharge phase) in the low density regime while the particles cannot grow larger than certain size (30 nm in our case) in the high density regime (they were diffused out from the chamber after 120 s).

In order to figure out which causes the fast growth rate in the high density regime, the measured particle size was compared with the modeling result based on the agglomeration model[17] to investigate different growth rates between low and high density regimes. In the model, agglomeration of a few nanometer-sized proto particles to the predator particle is responsible for the particle growth. The time derivative of the particle radius r_p is expressed as[17]

$$\frac{dr_p}{dt} = \left(\frac{v_{th,0}}{4\rho_0}\right)\left[n_pm_0 + \rho_0't - n_pm_0\left(\frac{r_p}{r_0}\right)^3\right], \quad (4)$$

where r_0 is the proto particle radius, $v_{th,0} = (3kT_0/m_0)^{1/2}$ is the thermal speed of the proto particle, m_0 and T_0 are the proto particle mass and temperature, respectively, ρ_0 is the proto particle mass density, ρ_0' is the constant creation rate of the proto particle mass density, and n_p is the constant nanoparticle number density. The proto particle temperature $T_0 = 1/40$ eV for simplicity based on the fact that the calculated results do not significantly depend on T_0. The solid curves in Fig. 3 indicate the modeling results obtained by using r_0 and ρ_0' as fitting parameters that produce the best fit of the measured data. As a result, while r_0 is almost same ($r_0 = 1$ nm) in both density regimes, $\rho_0' = 1.2\times10^{-7}$ kg/m^{3}s for the low density plasma and $\rho_0' = 3.3\times10^{-7}$ kg/m^{3}s for the high density plasma. It means that the fast agglomeration growth in the high density plasma is attributed to the high proto particle creation rate ρ_0'.

In general, the growth rate of the agglomeration step is temporally nonlinear while that of the molecular accretion step is temporally linear.[18] Therefore, we can conclude that

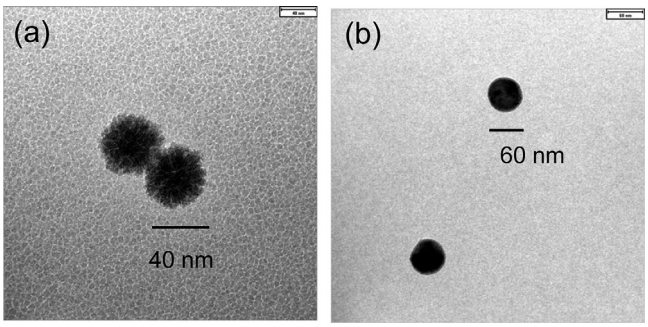

FIG. 4. Morphology of the nanoparticles at (a) 100 W and (b) 200 W. The nanoparticle shape is spherical in the high n_i regime due to the rearrangement of atoms by surface heating of the particle, and it is cauliflower-like in the low n_i regime due to the agglomeration growth.

the molecular accretion step did not take place in high density regime while it occurred in low density regime. The reason for missing of the molecule accretion step is related to the nanoparticle transport. Most of the nanoparticles are levitated in the plasma edge region due to the particle transport while the main sources for molecular accretion growth of nanoparticles, SiH_2 and SiH_3 radicals, are actively generated and exist in the bulk plasma region.[19] Consequently, the nanoparticles have little chance to encounter the SiH_2 and SiH_3 radicals, and this is why the molecular accretion growth is not observed in the high density regime.

The morphology of the generated nanoparticles depicted in Figs. 4(a) and 4(b) demonstrates the cauliflower-like and smooth spherical shapes in the low and high density regimes, respectively. This discrepancy is observed from all the images we took. The cauliflower-like nanoparticles is commonly observed in the previous results of the capacitively coupled plasma[18] and is induced by agglomeration growth. On the other hand, the spherical nanoparticles in the high density regime are related to the crystallization. In general, the nanoparticle immersed in the plasma is heated by ion impact and *e-i* recombination at the nanoparticle surface. The nanoparticles can be also heated by Si_xH_y radicals but the energy transfer rate between a nanoparticle and a radical is much less than that between a nanoparticle and an ion. The photon flux is also negligible at the power level of the laser under experiment (<30 mW). On the other hand, it is cooled down by collisions with cold neural gas (in low temperature plasma) and by emitting thermal radiation. Our calculation of the 20 nm radius nanoparticle temperature based on Ref. 20 shows 1520 K for the high density regime, which may be sufficiently high for the crystallization of nano-sized silicon particles although the melting temperature of the nano-sized material is known to be lower than that of the bulk material (1700 K).[21] In comparison, the nanoparticle temperature for the low density regime is 337 K. We also observed that most of the nanoparticles generated in high density regime have a crystalline structure seen by the high resolution TEM images.

In the high ion density plasma, the produced nano-sized dust particles exhibit a large difference in the growth, transport, and morphology compared with those in the low ion density plasma, showing the strong transport toward the chamber wall and the crystallization. In addition, the molecular accretion does not take place due to the particle transport, and the growth rate of the agglomeration step is shown to be high because of the high proto (or seed) particle creation rate. Compared to the low density plasma, the problems brought about by dust particles, such as reduction of product yield and decline of plasma performance, may be less serious in the high density plasma due to the smaller final particle size and their spatial residence at the plasma edge. The plasma parameters are more or less unchanged over time in the high density plasma. Our results also suggest that high density plasma is favorable for the synthesis of highly crystalline nanoparticles because of the high ion flux.

This work was supported by National R&D Program through the National Research Foundation of Korea (NRF) funded by the Ministry of Education, Science and Technology (Grant No. 2012-0005923). The authors would like to thank Mr. Hyo-Chang Lee for his experimental assistance.

[1]C. K. Goertz, Rev. Geophys. **27**, 271 (1989).
[2]H. Thomas, G. E. Morfill, V. Demmel, J. Goree, B. Feuerbacher, and D. Mohlmann, Phys. Rev. Lett. **73**, 652 (1994).
[3]J. Winter and G. Gebauer, J. Nucl. Mater. **266–269**, 228 (1999).
[4]B. J. Hinds, T. Yamanaka, and S. Oda, J. Appl. Phys. **90**, 6402 (2001).
[5]Y. Watanabe, M. Shiratani, Y. Kubo, I. Ogawa, and S. Ogi, Appl. Phys. Lett. **53**, 1263 (1988).
[6]P. K. Shukla and B. Eliasson, Rev. Mod. Phys. **81**, 25 (2009).
[7]U. Kortshagen, J. Phys. D: Appl. Phys. **42**, 113001 (2009).
[8]S. Hong, C. Grisolia, V. Rohde, P. Monier-Garbet, Tore Supra Team, and ASDEX Upgrade Team, Nucl. Fusion **50**, 035002 (2010).
[9]S. A. Khrapak, A. V. Ivlev, G. E. Morfill, and H. M. Thomas, Phys. Rev. E **66**, 046414 (2002).
[10]I. B. Denysenko, K. Ostrikov, S. Xu, M. Y. Yu, and C. H. Diong, J. Appl. Phys. **94**, 6097 (2003).
[11]K. B. Chai, C. R. Seon, C. W. Chung, N. S. Yoon, and W. Choe, J. Appl. Phys. **109**, 013312 (2011).
[12]M. H. Lee, S. H. Jang, and C. W. Chung, J. Appl. Phys. **101**, 033305 (2007).
[13]K. B. Chai, C. R. Seon, S. Park, and W. Choe, New J. Phys. **11**, 103006 (2009).
[14]T. Matsoukas and M. Russell, J. Appl. Phys. **77**, 4285 (1995).
[15]J. Perrin, P. Molinas-Mata, and P. Belenguer, J. Phys. D **27**, 2499 (1994).
[16]M. A. Lieberman and A. J. Lichtenberg, *Principles of Plasma Discharges and Materials Processing* (Wiley, New York, 1994).
[17]D. S. Lemons, R. K. Keinigs, D. Winske, and M. E. Jones, Appl. Phys. Lett. **68**, 613 (1996).
[18]L. Boufendi and A. Bouchoule, Plasma Sources Sci. Technol. **3**, 262 (1994).
[19]M. Hertl and J. Jolly, J. Phys. D: Appl. Phys. **33**, 381 (2000).
[20]A. Bouchoule, *Dusty Plasmas—Physics, Chemistry and Technological Impact in Plasma Processing* (Wiley, New York, 1999), p. 20.
[21]P. Buffat and J. P. Borel, Phys. Rev. A **13**, 2287 (1976).